

Article

# Impacts of Climate Change on Rainfall Erosivity in the Huai Luang Watershed, Thailand

Plangoen Pheerawat <sup>1,\*</sup> and Parmeshwar Udmale <sup>2</sup> 

<sup>1</sup> Department of Civil Engineering, Faculty of Engineering, Siam University, 38 Petchkasem Road, Phasi Charoen District, Bangkok 10160, Thailand

<sup>2</sup> Department of Civil and Earth Resources Engineering, Graduate School of Engineering, Kyoto University, Room 132, C1, Kyoto-Daigaku-Katsura, Nishikyo-ku, Kyoto 615-8540, Japan; pd.udmale@gmail.com

\* Correspondence: pheerawat.pla@siam.edu

Received: 14 June 2017; Accepted: 4 August 2017; Published: 6 August 2017

**Abstract:** This study focuses on the impacts of climate change on rainfall erosivity in the Huai Luang watershed, Thailand. The multivariate climate models (IPCC AR5) consisting of CCSM4, CSIRO-MK3.6.0 and MRI-CGCM3 under RCP4.5 and RCP8.5 emission scenarios are analyzed. The Quantile mapping method is used as a downscaling technique to generate future precipitation scenarios which enable the estimation of future rainfall erosivity under possible changes in climatic conditions. The relationship between monthly precipitation and rainfall erosivity is used to estimate monthly rainfall erosivity under future climate scenarios. The assessment compared values of rainfall erosivity during 1982–2005 with future timescales (i.e., the 2030s, 2050s, 2070s and 2090s). The results indicate that the average of each General Circulation Model (GCM) combination shows a rise in the average annual rainfall erosivity for all four future time scales, as compared to the baseline of 8302 MJ mm ha<sup>-1</sup> h<sup>-1</sup> year<sup>-1</sup>, by 12% in 2030s, 24% in 2050s, 43% in 2070s and 41% in 2090s. The magnitude of change varies, depending on the GCMs (CCSM4, CSIRO-MK3.6.0, and MRI-CGCM3) and RCPs with the largest change being 82.6% (15,159 MJ mm ha<sup>-1</sup> h<sup>-1</sup> year<sup>-1</sup>) occurring under the MRI-CGCM3 RCP8.5 scenario in 2090s. A decrease in rainfall erosivity has been found, in comparison to the baseline by 2.3% (8114 MJ mm ha<sup>-1</sup> h<sup>-1</sup> year<sup>-1</sup>) for the CCSM4 RCP4.5 scenario in 2030s and 2.6% (8088 MJ mm ha<sup>-1</sup> h<sup>-1</sup> year<sup>-1</sup>) for the 2050s period. However, this could be considered uncertain for future rainfall erosivity estimation due to different GCMs. The results of this study are expected to help development planners and decision makers while planning and implementing suitable soil erosion and deposition control plans to adapt climate change in the Huai Luang watershed.

**Keywords:** climate change; rainfall erosivity; precipitation; soil erosion; sedimentation

## 1. Introduction

Rainfall erosivity (R factor) represents a measure of the erosive force of rain or its potential to cause soil erosion. The R factor of the Revised Universal Soil Loss Equation (RUSLE) [1] is a useful tool for identifying areas with high soil loss potential and thereby determining area specific soil conservation structures. The R factor quantifies the impact of rainfall and reflects the amount and rate of runoff that can be associated with soil erosion. The rainfall erosivity for a given storm as per USLE [2] or its revised version, RUSLE [1] is equal to the product of the total storm energy (E) and the maximum 30-min rainfall intensity (I<sub>30</sub>). However, the use of EI<sub>30</sub> alone is not sufficient to describe the relative rainfall erosivity [3]. Moreover, it requires continuously recorded rainfall data which is not commonly available in remote areas. Thus, an index based on kinetic and momentum of run-off can also be used to estimate the monthly or annual values of rainfall erosivity with accurate record

usually available for an extended period. Till date, many indices which relate the erosivity to soil loss estimation have been established (such as Diodato, et al. 2004 [4], Diodato and Bellochi 2007 [5], Angulo-Martínez et al. 2009 [6], Hernando and Romana 2015 [7]). However, most of the studies have application to a particular geographical location and area. The most widely used index is the Fournier index [8]. It has been found to have a good relationship with annual values of rainfall erosivity. However, this Fournier index has shortcomings and subsequently modified into Modified Fournier Index (MFI) [9]. This modified index is summed for a whole year and found to be linearly correlated with EI<sub>30</sub> index of the USLE [10].

Global changes in precipitation and temperature patterns are expected to impact soil erosion through multiple pathways, including changes in rainfall erosivity [11]. Climate change is expected to affect soil erosion based on a variety of factors, including precipitation amounts and intensities, temperature impact on soil moisture and plant growth [12]. The erosive power of rainfall has a direct effect on soil loss. Current general circulation models (GCMs) and regional climate models (RCMs) [13,14] cannot provide detailed precipitation information that enables the determination of the extent of rainfall erosivity directly as a function of rainfall kinetic energy and rainfall intensity. Climate change is expected to impact soil erosion based on factors like precipitation amount, the impact of precipitation intensity on soil moisture and plant growth [15]. The most direct effect of climate change on erosion by water can be expected to be the effect of changes in rainfall erosivity [16–19]. Thus, an increase in soil erosion can be expected due to the increase in rainfall erosivity. Table 1 shows earlier studies projecting impacts of climate change on rainfall erosivity [19–23]. Climate change is expected to affect soil erosion based on a variety of factors [24] including changes in precipitation amount and intensity, impacts on soil moisture and plant growth, etc. Several studies have also shown that climate change could significantly affect soil erosion (as shown in Table 2) [19,20,25,26]. One of the direct impacts of climate change on soil erosion is the change in the erosive power of rainfall [23–25]. The contribution of water as an eroding agent can be represented by rainfall erosivity (R-factor). This factor is important and dominant in the Universal Soil Loss Equation (USLE) and the Revised Universal Soil Loss Equation (RUSLE). Both USLE and RUSLE are sets of mathematical equations that estimate average annual soil loss from interrill and rill erosion [27].

Zhang et al. (2010) [20] have illustrated that the projected increases in future rainfall erosivity forewarn important trends of soil loss and runoff in the northeastern China. Based on the USLE or RUSLE estimates, a 1% increase in rainfall erosivity will cause a 1% increase in soil loss assuming other factors related to crops, management, and conservation practices remain the same. The expected increase in erosivity will impose more pressure on the land resources and may have a significant negative impact on agricultural production. The study highlights the need to design, plan and implement soil conservation practices to combat potentially severe soil erosion in this region under climate change.

Panagos et al. (2015) [28] have recommended that rainfall erosivity equations should be used with caution in various applications. The rainfall erosivity empirical relationships developed are location specific and, in most cases, those relationships cannot be applied to other regions or over larger areas (Panagos et al., 2015, Oliveira et al., 2013) [29,30]. Also, empirical equations cannot capture the impact of high rainfall intensities on the average rainfall erosivity. Prassanakumar et al. (2009) [30] suggest that information on soil erosion on a sub-watershed scale contributes significantly to the planning for soil conservation, erosion control, and management of the watershed environment. In this background, it is important to develop a relationship between rainfall and erosivity at specific locations or the watershed level using available data. The present study aims to establish an empirical relationship between rainfall and erosivity using observed rainfall data and based on estimated empirical relationship, to estimate the future rainfall erosivity under the influence of climate change at the local scale (the Huai Luang watershed located in the northeastern Thailand). The outcomes of this study are expected to be useful to policy makers to plan various soil erosion control practices in the watershed.

**Table 1.** Previous studies about impacts of climate change on rainfall erosivity.

Authors	Study area and Location	Climate Models	Climate Scenarios	Baseline Period	Projected Period	Projected Change in Precipitation (%)	Projected Change in Rainfall Erosivity (%)
Zhang et al., 2010 [20]	Northeast of China	CGCM3.1 (T47) CGCM3.1 (T63) CSIRO-MK3.0 UKMO-HadCM3 UKMO-HadGEM1 ECHAM5/MPI-OM	A2, A1B, B1	1960–1999	2030–2059 2070–2099	+13.33 +21.33	+54.33 +73.66
Shiono et al., 2013 [21]	Hokkaido Island, Japan	RCM20	A2	1995–2009	2031–2050 2081–2100	+30 +8	+26 +23
Plangoen et al., 2014 [10]	Upper Nan Watershed, Thailand	PRECIS: ECHAM4, GFDLR-30, HadCM3 and CCSM3	A2,B2,A1B, B1	1971–2000	2011–2040	+2.14	+5.02
					2041–2070	+5.19	+10.32
					2071–2099	+7.00	+14.20
Hoomehr et al., 2016 [22]	Southern Appalachian region, USA	CCSM	A1FI, A1B, B1	1959–2000	2010–2099	+3 to +12	+7 to +19
Panagos et al., 2017 [23]	EUROPE	HadGEM2	RCP4.5	2010s	2050s	-	–23.9 to 78.2

**Table 2.** Previous studies of impacts of projected climate change on soil erosion in Asian case using RUSLE and USLE.

Year	Author(s)	Country/Region	Erosion Models	Climate Models	Climate Scenarios
2010	Zhang et al. [20]	Northeast China	RUSLE	CGCM3.1 (T47),CGCM3.1 (T63), CSIRO-MK3.0, UKMO-Hadcm3, UKMO-HadGEM1, ECHAM5/MPI-OM	A2, A1B, B1
2011	Park et al. [25]	All land areas of Korea	RUSLE	Mesoscale Model Version 5	A1B
2013	Plangoen et al. [19]	Mae Nam Nan sub-catchment, Thailand	RUSLE	CCSM3 HadCM3 PRECIS RCM	A2, A1B, B1
2015	Mondal et al. [26]	Narmada River Basin, India	USLE	HADCM3	A2

Deforestation has been steadily occurring over the past century due to an increase in the area under upland crop cultivation in northeastern Thailand [31] (LDD, 2005). There was an increase in the cultivation of cash crops such as cassava, sugarcane and maize and this cultivation expanded to the highlands of the Huai Luang watershed. Due to deforestation, intensive land uses and the topography, soil erosion has become a major environmental problem in the Huai Luang watershed. Soil erosion affects crop productivity and soil fertility, both of which are leading to lower incomes for farmers and insufficient food production for the ethnic minority populations in the study area. The rate of soil erosion in the northeast Thailand, on an average, is higher than  $150 \text{ ton ha}^{-1} \text{ year}^{-1}$  [31] (LDD, 2005). Soil erosion leads not only to long-term losses in crop productivity but also causes a reduction in the storage capacity of reservoirs, which in turn leads to increased flooding and reduced irrigation capacity downstream. For the past few decades, encroachment of agricultural activities on forest areas and the misuse of land have become serious problems in the Huai Luang watershed. Thailand Research Fund (TRF) initiated a climate change research program and provided funding to support the development of climate change scenarios in the northeast Thailand to use in subsequent impact assessments studies [32]. Most of the 8 GCMs (CCMA CGCM3.1, MPI\_ECHAM5, GISS, CNRM\_CM3, CSIRO\_MK3.0, CSIRO\_MK3.5, IPSL\_CM4, and GFDL\_CM2.0) show that the average monthly maximum temperature in northeast Thailand is expected to increase by  $3 \text{ }^{\circ}\text{C}$ – $4 \text{ }^{\circ}\text{C}$  and the average monthly minimum temperature is expected to increase by over  $4 \text{ }^{\circ}\text{C}$  throughout the country. Also, the Northeastern plateau tends to have unchanged annual precipitation, with the potential for slightly higher precipitation during the dry season and slightly lower precipitation during the late part of the rainy season.

## 2. Materials and Methods

### 2.1. Materials

#### 2.1.1. Study Area

The Huai Luang watershed is located in Udon Thani province of the northeast Thailand (Figure 1). The watershed covers about  $3428 \text{ km}^2$  area with the highest elevation of 567 meters above mean sea level (m amsl) (elevation range of 631–153 m amsl). The main river—The Huai Luang—is a tributary of the Mekong River. The watershed has hilly and rolling hill topography in the south and north regions, pen plain morphology at the central to northeast side and along the Huai Luang River with the low elevation of 87 m amsl. The land use land cover (LULC) map is modified from the map constructed by the Land Development Department [33]. Nine classes of LULC are mapped as follows: orchard, cassava, maize, forest, paddy field, pasture, sugarcane, urban, and water body (Figure 1). Paddy field occupies about 40% of the area. The orchard is grown in the northwest to southwest regions covering an area of about 9%. Water bodies, urban area, and forest area covers about 5%, 8% and 17% of the watershed area, respectively.

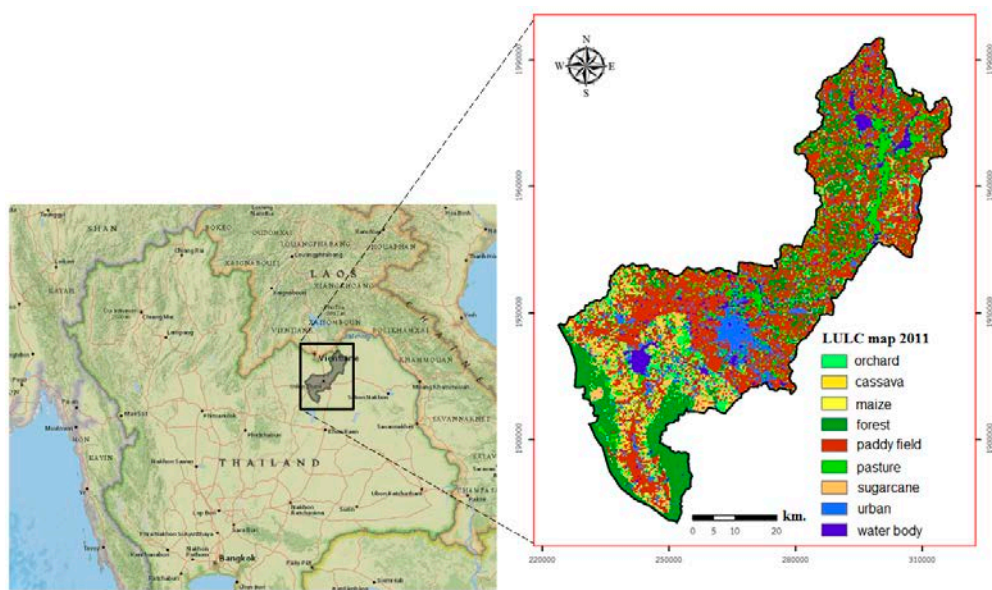


Figure 1. Location of the Huai Luang watershed.

### 2.1.2. Soil Series

The major soil series in the watershed is Nong Bunnak (Nbn), Phon Ngam (Png), Phon Phisai (Pp), Bua Lai (Bli), Dan Sai (Ds), Lam Thamenchai (Ltc), and Chakkarat (Ckr) [34]. The Ds series covers a relatively large area of the watershed (about 23.94%). The soil series are characterized based on their saturated hydraulic conductivity values into three groups, namely, slow, moderate, and rapid soils. The slow soils (Pp, Nbn) are soils having very less infiltration rates ( $<5 \times 10^{-7}$  m/s), mainly consist of clay soils, silty clay soil over nearly impervious material. The moderate soils (Bli, Ds, Ckr) are soils having moderate infiltration rates ( $5 \times 10^{-7}$  to  $5 \times 10^{-6}$  m/s), moderately well-drained soils with fine to moderately fine textures such as loam, sandy clay loam. The rapid soils (Png, Ltc) are soils having high infiltration rates ( $>5 \times 10^{-6}$  m/s) are excessively well-drained such as loamy sand and sand. About 52% of the Huai Luang watershed area is covered with moderately infiltrated soil series type (Figure 2).

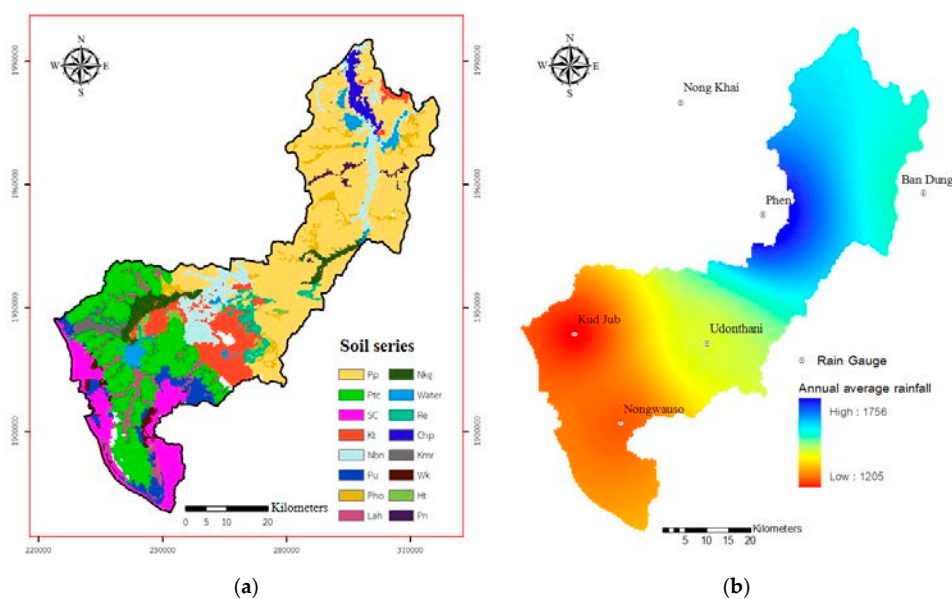
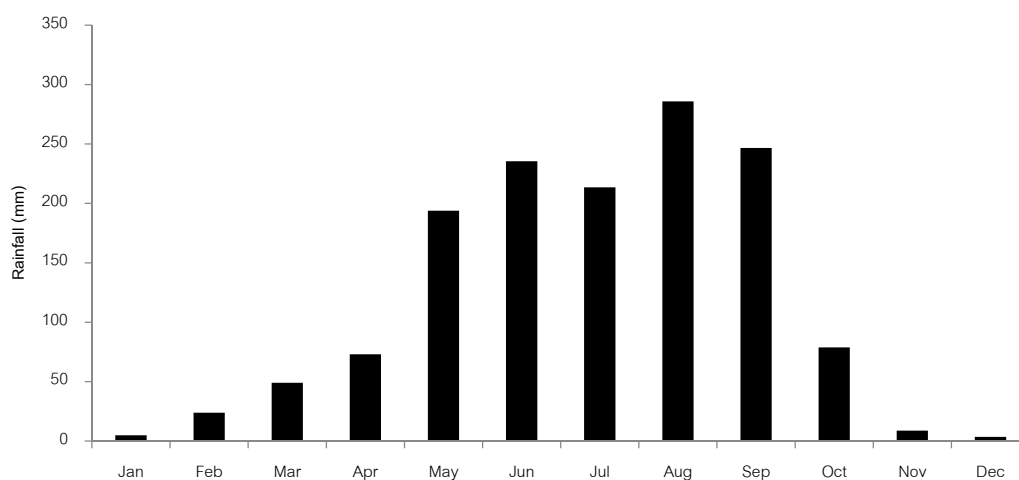


Figure 2. (a) Soil series and (b) location of rain gauge stations in the Huai Luang Watershed.

### 2.1.3. Climate

The climate in the Huai Luang basin is tropical, characterized by winter, summer, and rainy seasons, and influenced by the Northeastern and Southwestern Monsoons. The rainy season brought by the Southwestern monsoon originating at the Indian Ocean lasts from the mid-May to the end of October. July and August are usually the months of intense rainfall. The winter season with cold and dry weather due to the Northeastern Monsoon begins in November and ends in February. From mid-February until mid-May, the weather is warm. The climate data from 1981 to 2010 (average 30 years) for this study are collected from the Thai Meteorological Department. The average annual rainfall is about 1250 mm. More than 80% (1000 mm) of the total rainfall is concentrated in the wet season only. Figure 3 shows the mean monthly rainfall and maximum and minimum air temperature in the watershed. The mean maximum monthly rainfall is about 285 mm observed in August and the mean minimum monthly rainfall of 3.5 mm observed in December. The minimum temperature varies between 16.26 °C and 24.97 °C and maximum temperature varies between 29.04 and 36.40 °C.



**Figure 3.** Observed climate data in the study area during 1981–2010.

## 2.2. Data and Methods

### 2.2.1. Observed Precipitation

The observed rainfall data is obtained from the Thai Meteorological Department (TMD), Thailand. There are six rainfall gauge stations (Figure 2a) installed in the Huai Luang Watershed, and the data collected from these stations provides continuous 10-min interval rainfall records. This data was used to calculate the maximum 30-min rainfall intensity ( $EI_{30}$ ) from 2000 to 2002. These stations also provided the daily rainfall data from 1981 to 2010.

### 2.2.2. Estimation of Rainfall Erosivity

In this study, the rainfall erosivity is determined over 2000 to 2002 to create a relationship between daily precipitation and daily  $EI_{30}$  by using the methodology described in [1,2]. Rainfall storm events of less than 12.7 mm were omitted from the rainfall erosivity calculation, unless at least 6.4 mm of rain dropped in 15 min. A storm period with less than 1.3 mm over 6 h was divided into two storms. The threshold of 12.7 mm is selected deliberately because it is a part of the criteria used to describe a storm for computing storm  $EI_{30}$  values and thus the R-factor [2]. These storms add little to erosivity and significantly reduce the quantity of rainfall data that must be processed [1]. Other studies have validated that changing the rainfall threshold from 12.7 mm to 0 mm increases rainfall erosivity by no more than 3.5% or 5% on average. Therefore, storms less than 12.7 mm are deleted when calculating erosivity for modern water erosion techniques such as RUSLE. Aforementioned has done to have

some influence on computing reduced erosion for lower rainfall amounts and intensities because of little or no runoff in such situations [35]. The concept of rainfall erosivity refers to the ability of any rainfall event to erode soil. Rainfall erosivity is defined as the average annual value of the rainfall erosion index [2]. The monthly rainfall erosivity value is computed by summing up  $EI_{30}$  values of storms that occur during a month. The RUSLE model uses the approach developed by Brown and Foster (1987) [36] to calculate the average annual rainfall erosivity,  $R$  ( $\text{MJ mm ha}^{-1} \text{ h}^{-1} \text{ year}^{-1}$ )

$$R = \frac{1}{n} \sum_{j=1}^n \left[ \sum_{k=1}^m E_k \cdot (I_{30})_k \right] \quad (1)$$

where,  $E$  is the total storm kinetic energy ( $\text{MJ ha}^{-1}$ );  $I_{30}$  is the maximum intensity of a 30 min rainfall ( $\text{mm h}^{-1}$ );  $j$  is the index of the number of years used to produce the average;  $k$  is the index of the number of storms in each year;  $m$  is the number of storms in each year; and  $n$  is the number of years. To calculate the erosivity index ( $EI_{30}$ ) value for a particular storm ( $\text{MJ ha}^{-1} \text{ mm}^{-1}$ ), the total storm kinetic energy ( $E$ ) ( $\text{MJ ha}^{-1}$ ) is multiplied by the maximum amount of rain falling within 30 consecutive minutes ( $I_{30}$ ) expressed in millimeters per hour units ( $\text{mm h}^{-1}$ ). The total storm kinetic energy ( $E$ ) is calculated using this relation:

$$E = \sum_{j=1}^m e_r \Delta V_r \quad (2)$$

where,  $e_r$  is the rainfall energy per unit rainfall depth area in megajoules per hectare per millimeter ( $\text{MJ ha}^{-1} \text{ mm}^{-1}$ );  $\Delta V_r$  is the depth of rainfall in millimeters (mm) for the  $r^{\text{th}}$  increment of the storm hyetograph divided into  $m$  parts, in which each part essentially has constant rainfall intensity.

Rainfall energy per unit depth of rainfall ( $e_r$ ) is calculated using this relation:

$$e_r = 0.29[1 - 0.72 \exp(-0.05i_r)] \quad (3)$$

where  $e_r$  is measured in the unit of  $\text{MJ ha}^{-1} \text{ mm}^{-1}$ , and  $i_r$  is rainfall intensity ( $\text{mm h}^{-1}$ ). A comparison of the revised unit energy relation results with those of the relation presented in the Agriculture Handbook No. 537 shows less than a 1% difference in the  $EI$  of some sample storms [31]. Rainfall intensity for a particular increment in a rainfall event ( $i_r$ ) is calculated using the following relation,

$$i_r = \frac{\Delta V_r}{\Delta t_r} \quad (4)$$

where,  $\Delta t_r$  is the duration of the increment over which rainfall intensity is considered to be constant in an hour (h), and  $\Delta V_r$  is the depth of rain falling (mm) during the increment.

The relationship between precipitation and R-factor obtained using the above methodology is used to estimate the daily R-factor over 1982–2005, which further aggregated to monthly scale. Finally, the relationship between monthly precipitation and monthly R-Factor is established.

### 2.2.3. General Circulation Models (GCMs)

The estimation of future climate change, as provided by General Circulation Models (GCMs), does not entail the type of detailed storm information that is needed to predict the changes in rainfall erosivity. Therefore, relationships between rainfall erosivity and monthly precipitation have to be developed and could be used to analyze the impact of climate change on rainfall erosivity [11,32]. In this study, the commonly used CCSM4, CSIRO-MK3 and MRI-CGCM3 under representative concentration pathway (RCP) 4.5 and 8.5 were chosen to generate future precipitation scenarios in order to enable the estimation of future rainfall erosivity under possible changes in climatic conditions (Table 3). A study by McSweeney et al. (2015) [37] has shown better performances of CCSM4, CSIRO-MK3, and MRI-CGCM3 in the South East Asia. These model details are given in Table 1.

**Table 3.** Details of the climate models used to downscale future precipitation for this study.

Model Center	Model Name	Resolution (°)	Scenario	Timescale	Temporal Resolution
National Center for Atmospheric Research	CCSM4	1.25 × 0.94	Historical, RCP 4.5 and RCP 8.5	Daily	1982–2005 2021–2040 (2030s) 2041–2060 (2050s) 2061–2080 (2070s) 2081–2100 (2090s)
Commonwealth Scientific and Industrial Research Organization in collaboration with Queensland Climate Change Centre of Excellence	CSIRO-MK3.6.0	1.875 × 1.875	Historical, RCP 4.5 and RCP 8.5	Daily	1982–2005 2021–2040 (2030s) 2041–2060 (2050s) 2061–2080 (2070s) 2081–2100 (2090s)
Meteorological Research Institute, Japan	MRI-CGCM3	1.1 × 1.1	Historical, RCP 4.5 and RCP 8.5	Daily	1982–2005 2021–2040 (2030s) 2041–2060 (2050s) 2061–2080 (2070s) 2081–2100 (2090s)

Several statistical downscaling techniques have been established to translate large-scale GCMs output into finer resolution [38]. In this study, the Bias correction method based on Quantile mapping is used to correct the precipitation projections. The correction of precipitation is more challenging compared to temperature as precipitation has many uncertainties. The non-parametric empirical Quantile method discussed in [39] is used to correct the daily precipitation. The concept of Quant is based on the following Equation (5),

A transformation factor ‘*h*’ is estimated that relates the model output variable to the observed variable such as:

$$P^{obs} = h(P^{GCMcon}) = 1/ECDF^{obs}(ECDF^{GCMcon}(P^{GCMcon})) \tag{5}$$

where,  $P^{obs}$  is observed precipitation;  $P^{GCMcon}$  is GCM simulated precipitation for control period;  $ECDF^{obs}$  is empirical cumulative distribution frequency (CDF) for the observed variable; and  $ECDF^{GCMcon}$  is Empirical CDF for control period generated by GCM. To calculate the value of ‘*h*’, the primary step should be estimation of probabilities of all the values in  $ECDF^{obs}$  and  $ECDF^{GCMcon}$  at a fixed interval of 0.01. Then only, ‘*h*’ could be estimated as the relative difference between the two ECDFs in each time slice. All calculations have been done using Qmap package of R.

### 3. Results and Discussion

#### 3.1. Estimation of Rainfall Erosivity (R-Factor) Using Observed Precipitation

The R-factor values of each rainfall station, as well as the mathematical formula that relates the R-factor values with rainfall, are developed based on historical rainfall data (2000–2002). These mathematical models are used to estimate the rainfall erosivity values of each rainfall station based on available monthly rainfall data. Table 4 presents R-factor and monthly rainfall ( $P_m$ ) values for each station. The power function gave the highest coefficient of determination during the comparison of the six stations. Simple regression is used for the analysis of monthly rainfall versus the monthly R factor. The regression equation had a 0.97 coefficient of determination for the Huai Luang watershed, which indicates its suitability in estimating the rainfall erosivity of the other meteorological stations (Figure 4). The resulting rainfall erosivity prediction models were assessed using a set of validation statistics that compared the observed and estimated values of the R factor (Figure 5).

**Table 4.** The developed R predictive models based on observed rainfall (1982–2005).

Station Name	Longitude (Eastings)	Latitude (Northings)	Annual Average Rainfall	R-Factor Model (MJ mm ha <sup>-1</sup> h <sup>-1</sup> year <sup>-1</sup> )
Udon Thani	102.48.00	17.23.00	1417.3	$R = 0.23P^{1.58}$ $r^2 = 0.98$
Phen	102.55.00	17.39.00	1786.3	$R = 0.25P^{1.58}$ $r^2 = 0.98$
Ban Dung	103.15.42	17.41.53	1504.7	$R = 0.36P^{1.52}$ $r^2 = 0.97$
Kud Jub	102.37.00	17.13.00	1205.0	$R = 0.51P^{1.45}$ $r^2 = 0.96$
Nong Wau So	102.37.00	17.13.00	1248.3	$R = 0.49P^{1.46}$ $r^2 = 0.95$
Nong Khai	102.44.00	17.52.00	1582.8	$R = 0.23P^{1.59}$ $r^2 = 0.98$
All 6 stations data				$R = 0.28P^{1.56}$ $r^2 = 0.97$

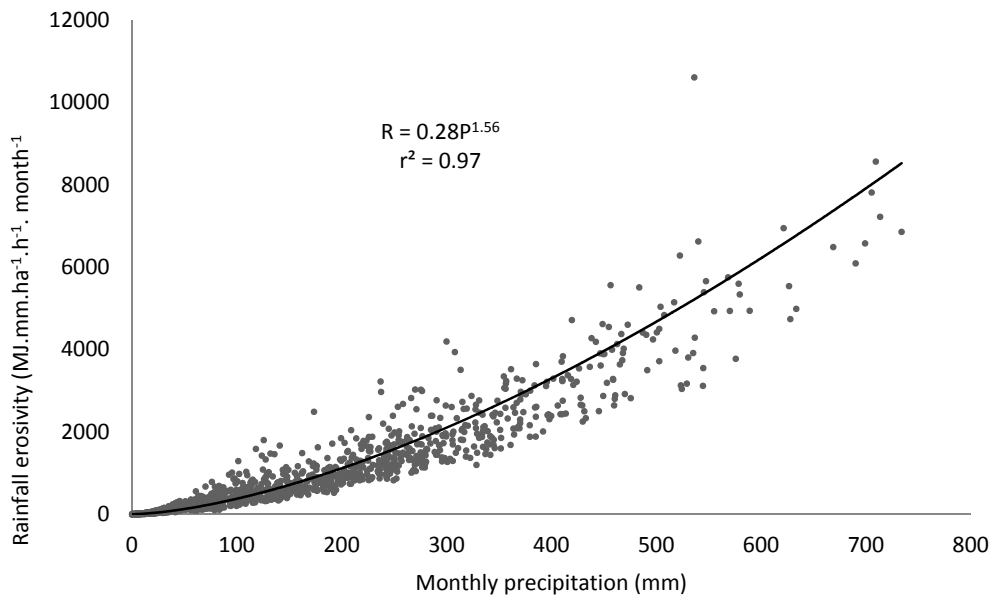


**Figure 4.** The relation between rainfall erosivity and monthly rainfall.

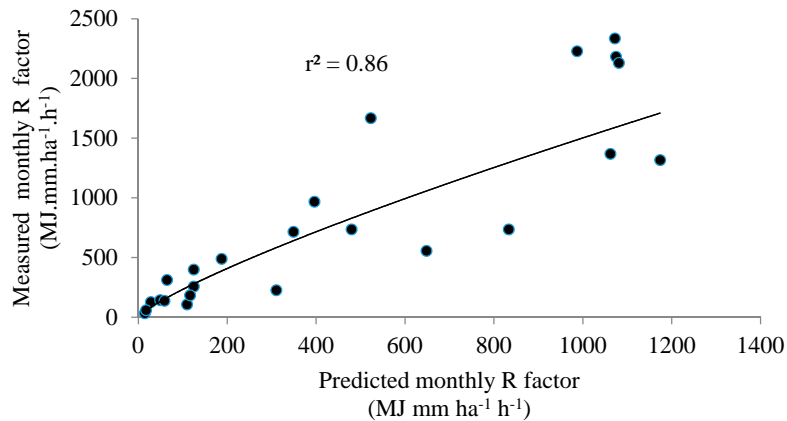


**Figure 5.** Scatter plot between predicted and estimated rainfall erosivity on the calibration data set.

This study examined the relationship between monthly rainfall and rainfall erosivity for six rain gauge stations in more detail and used Equations (1)–(4) in order to determine monthly and annual rainfall erosivity. The results of the calculations of rainfall erosivity factor values are listed in Table 5. Considerable differences in erosivity values were detected throughout the six rain gauge stations. It can be seen that the Phen station showed the highest erosivity value (11,824 MJ mm ha<sup>-1</sup> h<sup>-1</sup> year<sup>-1</sup>). On the other hand, the Nong Wau So station had the lowest value (7077 MJ mm ha<sup>-1</sup> h<sup>-1</sup> year<sup>-1</sup>). The R values varied among the stations as a result of the rainfall depths and regional features determined by elevation.

**Table 5.** Monthly rainfall erosivity for six rain gauge stations during 1982–2005 (Unit: MJ mm ha<sup>-1</sup> h<sup>-1</sup> month<sup>-1</sup>).

Code	354201	354001	354005	354008	354009	352201	All 6 Stations
Station	Udon Thani	Phen	Ban Dung	Kud Jub	Nong Wau So	Nong Khai	Average
Jan	11	19	16	13	4	24	15
Feb	84	82	105	107	64	53	83
Mar	258	194	200	176	133	138	183
Apr	416	644	501	341	579	391	479
May	1104	1632	1205	1026	784	1198	1158
Jun	1419	2228	1827	1195	958	1608	1539
Jul	1397	1746	1740	1092	1155	1732	1477
Aug	1754	2767	2538	1540	1734	1901	2039
Sept	1411	1975	1702	1447	1258	1456	1542
Oct	341	480	175	294	379	423	349
Nov	18	31	24	32	24	29	26
Dec	7	24	4	0	4	13	9
Annual *	8220	11,824	10,036	7261	7077	8967	8898

Note: \*—Unit for annual R is MJ mm ha<sup>-1</sup> h<sup>-1</sup> year<sup>-1</sup>.

### 3.2. Impact of Climate Change on Precipitation

Figure 6 presents the average monthly precipitation cycle for all climate projections in the four future scales and the baseline period (1982 to 2005). Overall, there is a dramatic rise in precipitation from January until it reaches its peak in August. After August, precipitation decreases significantly until December. It is clear that the precipitation peak range in August of climate projections is between 257–332 mm in 2030s, 219–350 mm in 2050s, 264–392 mm in 2070s and 259–434 mm in 2090s. Table 6 presents individual model-projected mean annual precipitation, and its changes averaged over the region during the four future periods under the RCP4.5 and RCP8.5 scenarios. All the models, except models CCSM4 under RCP4.5 scenario for the 2030s and CCSM4 under RCP8.5 for the 2050s, projected increases in precipitation over the watershed. The average annual precipitation for all four future time periods increases from a baseline (1981–2010) of 1417 mm by about 6.4% (to 1282.1 mm) for 2030s, 14.6% (to 1623.9 mm) for 2050s, 26.7% (to 1795.9 mm) for 2070s and around 25.0% (to 1772.7 mm) for 2090s. Overall, the model CSIRO-MK3 under RCP8.5 scenario simulated the highest increase in mean precipitation during the period of the 2070s, while CCSM4 under RCP4.5 scenario projected the largest decrease of approximately –4.0% (1360.4 mm) for 2030s.

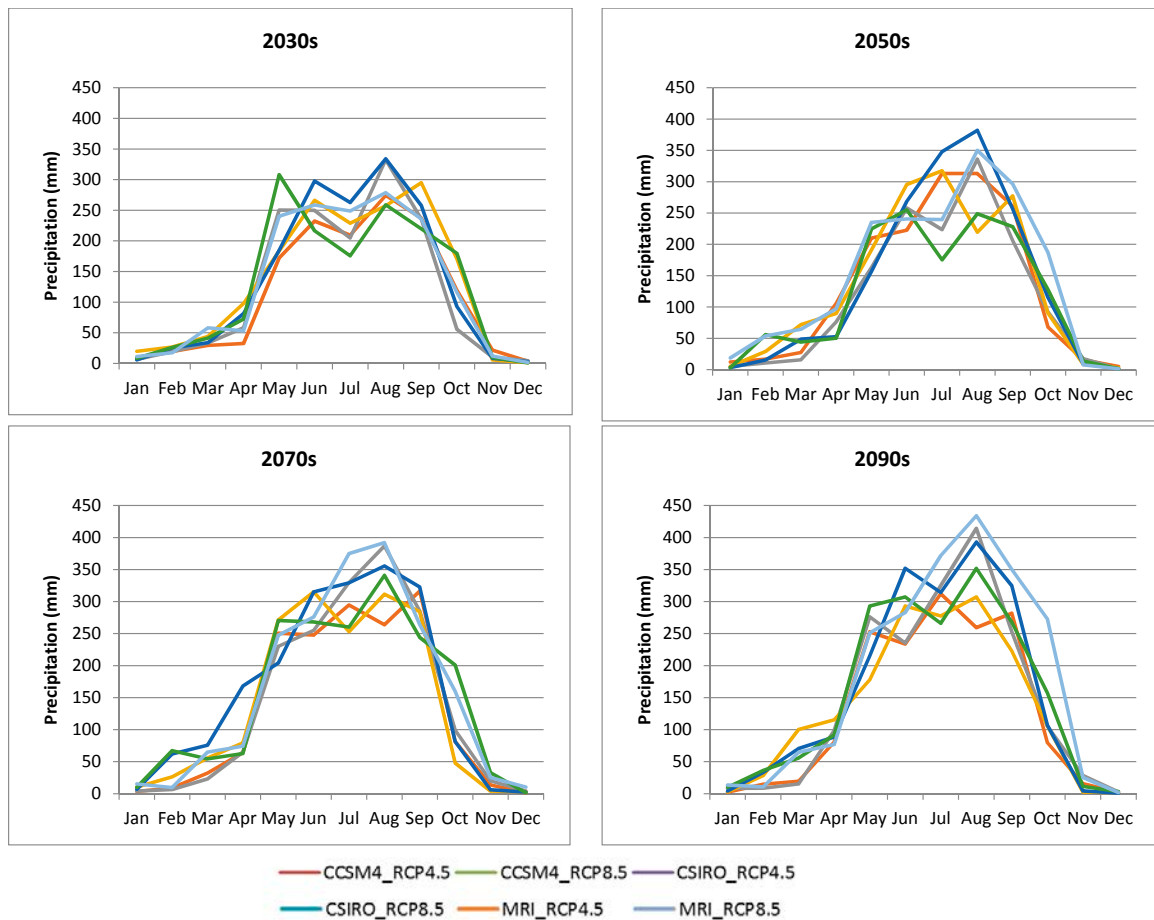


**Figure 6.** Average monthly precipitations for all climate projections for the 2030s, 2050s, 2070s, 2090s periods and the baseline period of 1982–2005.

**Table 6.** Annual average precipitations for climate projections compared to the baseline period, 1417 mm (1982–2005).

GCM	Scenario	2030s		2050s		2070s		2090s	
		Rainfall (mm)	Change (%)						
CCSM4	RCP4.5	1360.4	−4.0	1560.0	10.1	1577.9	11.3	1554.8	9.7
	RCP8.5	1460.7	3.1	1405.5	−0.8	1708.7	20.6	1631.8	15.1
CSIRO-MK3	RCP4.5	1595.9	12.6	1598.2	12.8	1793.5	26.5	1634.6	15.3
	RCP8.5	1587.1	12.0	1684.9	18.9	1968.8	38.9	1808.5	27.6
MRI-CGCM3	RCP4.5	1517.5	7.1	1428.1	0.8	1812.4	27.9	1851.5	30.6
	RCP8.5	1531.6	8.1	2066.9	45.8	1914.6	35.1	2155.4	52.1
Average		1282.1	6.4	1623.9	14.6	1795.9	26.7	1772.7	25.0

Figure 7 presents the precipitation change in the wet and dry seasons for all climate projections in the four periods and the baseline period (1982 to 2005). In general, there is a change in precipitation of all climate projections in the wet season (May to October); between −10 to 175 mm in 2030s, 6 to 424 mm in 2050s, 200 to 461 mm in 2070s and 130 to 709 mm in 2090s. Overall, the model MRI under RCP8.5 scenario predicted the highest increase in precipitation in the wet season during the period of 2050s, 2070s and 2090s while CCSM4 under RCP4.5 scenario projected the highest decrease approximately −10 mm for 2030s.

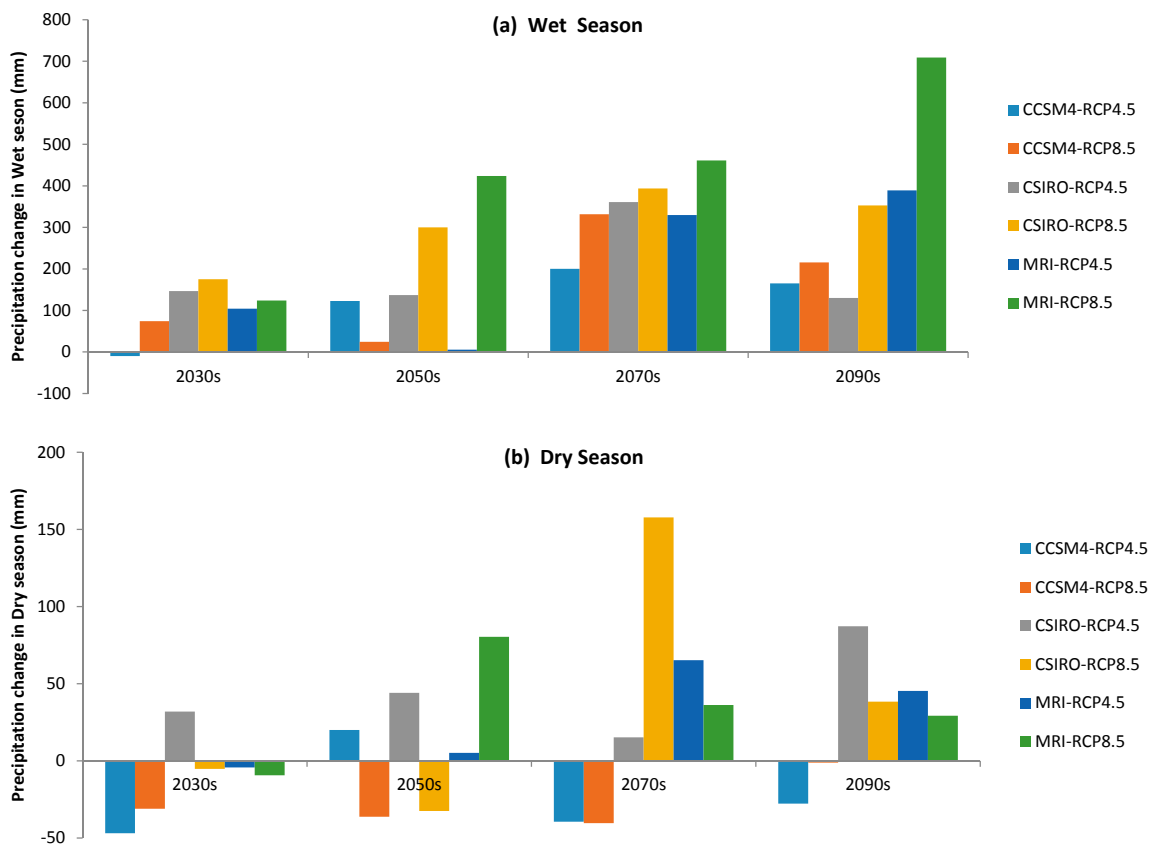


**Figure 7.** Precipitation change in (a) wet and (b) dry season for all climate projections for 2030s, 2050s, 2070s, and 2090s.

### 3.3. Impact of Climate Change on Rainfall Erosivity

The relationship between monthly precipitation and rainfall erosivity is used to predict rainfall erosivity values by equations ( $R = 0.28P^{1.56}$ ), as shown in Figure 4. One of the main objectives of this study is to predict rainfall erosivity under future climate scenarios, based on GCMs outputs consisting of CCSM4, CSIRO-MK3, and MRI-CGCM3 under RCP 4.5 and 8.5 scenarios. The use of multiple GCMs and RCP scenarios helps to address uncertainties inherent to models reliant on climatic factors. Table 7 presents the impact of climate change on annual rainfall erosivity in the Huai Luang watershed. The average of each GCM combination shows a rise in the average annual rainfall erosivity for all four future time periods. While the baseline value is  $8302 \text{ MJ mm ha}^{-1} \text{ h}^{-1} \text{ year}^{-1}$ , the increase ranges from 12% ( $9269 \text{ MJ mm ha}^{-1} \text{ h}^{-1} \text{ year}^{-1}$ ) in 2030s to 43% ( $11,854 \text{ MJ mm ha}^{-1} \text{ h}^{-1} \text{ year}^{-1}$ ) in 2070s. The magnitude of change varies, depending on the GCMs and RCPs with the largest change being 82.59% ( $15,159 \text{ MJ mm ha}^{-1} \text{ h}^{-1} \text{ year}^{-1}$ ) occurring under the MRI-CGCM3 under RCP8.5 scenario in 2090s. Also, there is a decrease in rainfall erosivity found as compared to the baseline of  $8302 \text{ MJ mm ha}^{-1} \text{ h}^{-1} \text{ year}^{-1}$ , from  $-2.29\%$  ( $8114 \text{ MJ mm ha}^{-1} \text{ h}^{-1} \text{ year}^{-1}$ ) for CCSM4 under RCP4.5 scenario in 2030s to  $-2.58\%$  ( $8088 \text{ MJ mm ha}^{-1} \text{ h}^{-1} \text{ year}^{-1}$ ) for the 2050s period.

**Table 7.** Annual rainfall erosivity and percent change for all climate projections compared to the base period (1982–2005).

Climate Models	GHGES	Annual Rainfall Erosivity (MJ mm ha <sup>-1</sup> h <sup>-1</sup> year <sup>-1</sup> )			Mean Change (%)	Stdev.
		Min	Max	Mean		
Base line		6530	11,363	8302	0.00	1343
2030s						
CCSM4	RCP4.5	6539	10,705	8114	−2.26	1266
	RCP8.5	7204	12,344	9280	11.78	1513
CSIRO-MK3.6.0	RCP4.5	7974	12,790	9858	18.74	1401
	RCP8.5	8074	13,108	10,109	21.77	1490
MRI-CGCM3	RCP4.5	7113	11,224	8893	7.12	1126
	RCP8.5	7377	12,248	9359	12.73	1405
Average		7380	12,070	9269	12	1367
2050s						
CCSM4	RCP4.5	8031	13,350	10,074	21.34	1538
	RCP8.5	6998	11,757	8866	6.79	1446
CSIRO-MK3.6.0	RCP4.5	7845	12,616	9808	18.14	1433
	RCP8.5	8678	14,089	11,025	32.80	1592
MRI-CGCM3	RCP4.5	6293	10,442	8088	−2.58	1126
	RCP8.5	11,210	17,233	14,009	68.74	1665
Average		8176	13,248	10,312	24	1467
2070s						
CCSM4	RCP4.5	8160	13,302	10,217	23.07	1530
	RCP8.5	8943	14,786	11,449	37.91	1685
CSIRO-MK3.6.0	RCP4.5	9561	16,445	12,506	50.64	1954
	RCP8.5	10,966	17,034	13,376	61.12	1844
MRI-CGCM3	RCP4.5	9060	14,618	11,390	37.20	1540
	RCP8.5	9757	15,313	12,187	46.80	1598
Average		9408	15,250	11,854	43	1692
2090s						
CCSM4	RCP4.5	8025	13,281	10,110	21.78	1608
	RCP8.5	8513	14,084	10,729	29.23	1570
CSIRO-MK3.6.0	RCP4.5	7869	12,976	10,045	20.99	1485
	RCP8.5	9552	15,407	12,042	45.05	1745
MRI-CGCM3	RCP4.5	9764	15,894	12,272	47.82	1736
	RCP8.5	12,247	19,086	15,159	82.59	1843
Average		9328	15,121	11,726	41	1665

Figure 8 shows that monthly rainfall erosivity changes under future climate are not in one direction for all GCMs (CCSM4, CSIRO, and MRI) under RCP4.5 and RCP8.5 scenarios. The intra-monthly patterns of rainfall erosivity changes range from the unimodal to the base line period. It is clear that this significant decrease in rainfall erosivity from November to February and an increase from March to October for all four time periods. Future changes in rainfall erosivity in comparison with the base period (8302 MJ mm ha<sup>-1</sup> h<sup>-1</sup>) is determined to be between 2.26 and 21.77% in 2030s, −2.58 and 68.74% in 2050s, 23.07 and 50.64% in 2070s and 20.99 and 82.59% in 2090s depending on GCMs and RCP scenarios.

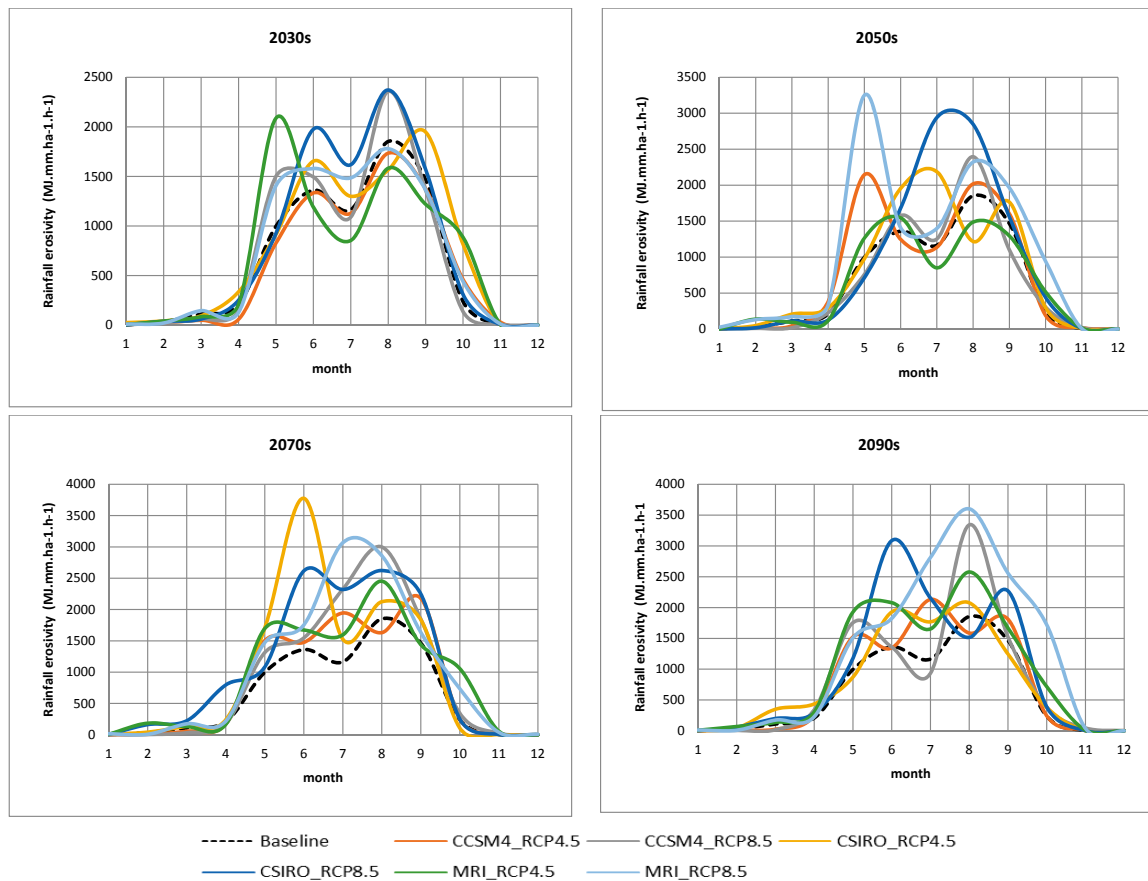


**Figure 8.** Rainfall erosivity for all climate projections for 2030s, 2050s, 2070s, 2090s and the baseline period (1982–2005) for the Huai Luang watershed.

Figure 9 illustrates the projected spatial patterns in rainfall erosivity changes using multivariate models (IPCC AR5) [7] under RCP4.5 and RCP8.5 scenarios for the four periods of 2030s, 2050s, 2070s and 2090s. The average of the three climate models under RCP4.5 scenarios shows that the average annual rainfall erosivity increases from the baseline rate of  $8302 \text{ MJ mm ha}^{-1} \text{ h}^{-1} \text{ yr}^{-1}$  by 7.9% for the 2030s, by 12.3% for the 2050s, by 37.0% for the 2070s and by 31.2% for the 2090s. The increase in the annual rainfall erosivity using average multivariate models (IPCC AR5) under RCP8.5 scenarios from the base line ( $8302 \text{ MJ mm ha}^{-1} \text{ h}^{-1} \text{ year}^{-1}$ ) was found to be 15.4% for the period of 2030s, 36.1% for the 2050s, 48.6% for the 2070s and 52.3% for the 2090s. It is clear that this significant increase in rainfall erosivity from baseline under RCP 4.5 and RCP8.5 scenarios for all periods. Projected rainfall erosivity increased over the most of the watershed. The models tended to project greater relative increases in rainfall erosivity in the northern compared to the southern watershed (Figure 9).

The results of present study are compared with Global Rainfall Erosivity database (Panagos 2017) [23]. According to this database, the range of rainfall erosivity over Thailand is found to be 2986 to  $13,253 \text{ MJ mm ha}^{-1} \text{ h}^{-1} \text{ year}^{-1}$ . Whereas, the range of R-factor over the Huai Luang watershed 6426 to  $9700 \text{ MJ mm ha}^{-1} \text{ h}^{-1} \text{ year}^{-1}$ . R-factors from presents study are in the range of  $7077\text{--}11,824 \text{ MJ mm ha}^{-1} \text{ h}^{-1} \text{ year}^{-1}$ . A previous study by Plangoen et al. (2013) have estimated the future rainfall erosivity in a watershed from Thailand in the range of 4866 to  $6384 \text{ MJ mm ha}^{-1} \text{ h}^{-1} \text{ year}^{-1}$  using the modified Fournier Index (MFI) and the R-factors using HadCM3 and PRECIS RCM under A2 and B2 scenarios and NCAR CCSM3 under A2, A1b and B1. However, in the present study, future rainfall erosivity ranged from 8114 to  $15,519 \text{ MJ mm ha}^{-1} \text{ h}^{-1} \text{ year}^{-1}$  by using a relationship between rainfall and erosivity based on CSSM4, CSIRO-MK3.6.0, and MRI-CGCM3 under RCP 4.5 and RCP8.5. This difference might have resulted from the differences in GCM and scenarios used.

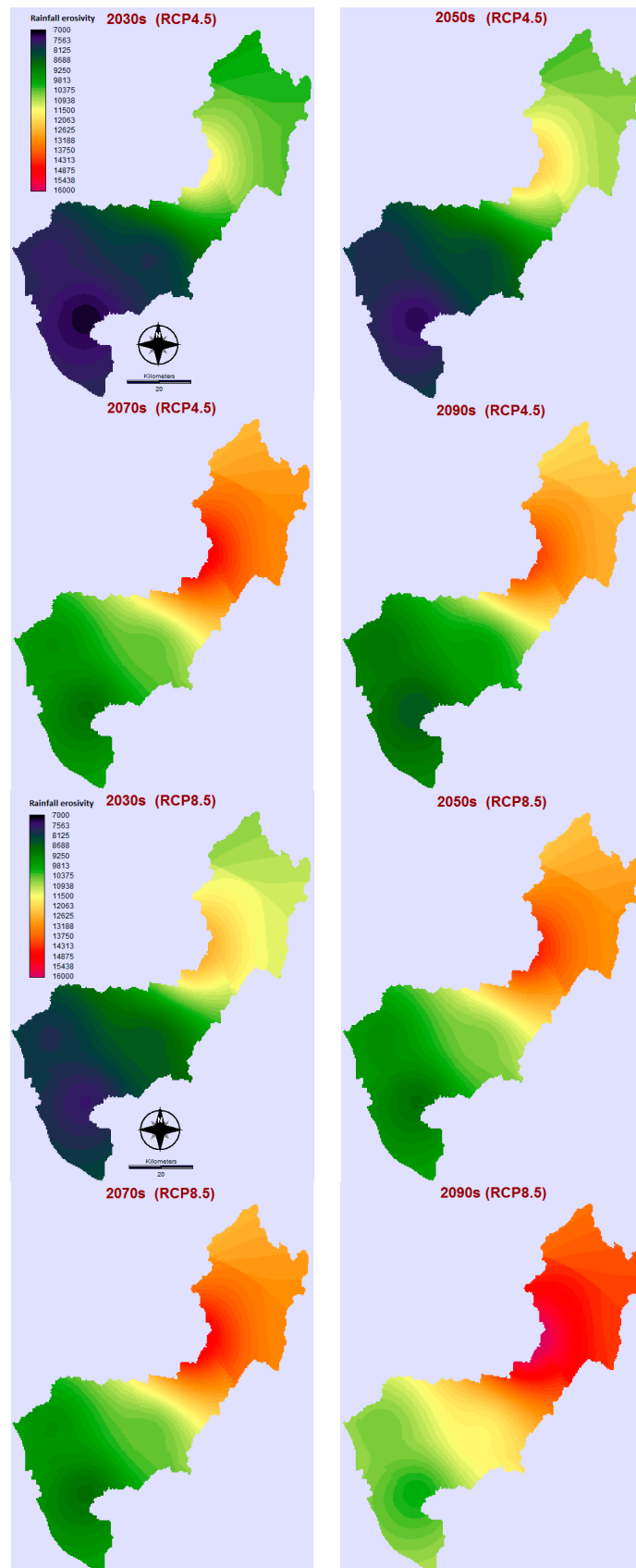


Figure 9. Rainfall erosivity maps using multivariate models under RCP4.5 ( $\text{MJ mm ha}^{-1} \text{h}^{-1} \text{year}^{-1}$ ).

#### 4. Conclusions

The use of multiple GCMs to estimate future rainfall erosivity helps to address the uncertainties inherent in global climate modeling as they provide a range of equally reasonable future climatic conditions. The present study uses multivariate models (CCSM4, CSIRO-MK3, and MRI-CGCM3) under RCP4.5 and RCP8.5 scenarios to predict average monthly and average annual rainfall erosivity in the Huai Luang watershed located in the Northeastern Thailand. The Quantile mapping method is used as a downscaling technique to generate future precipitation data. Future rainfall erosivity estimated by using the relationship between monthly precipitation and monthly rainfall erosivity. The results of this study showed a significant increase in annual rainfall erosivity using three general circulation models under RCP4.5 and RCP8.5 scenarios for the four periods. The expected increase in rainfall erosivity may have significant effects on soil erosion in the watershed, with projected changes in precipitation and rainfall erosivity causing increased soil loss in the future; proper strategies must be developed to tackle the possible increase in soil erosion and sediment deposition in the Huai Luang reservoir. The results of this study are expected to help development planners and decision makers when planning and implementing suitable soil erosion control plans to adapt climate change in Huai Luang watershed.

**Acknowledgments:** The research is financially supported by Thailand Research Fund (TRF). Authors are thankful to the Southeast Asia START Regional Center and Thai Meteorological Department (TMD) for providing the precipitation data. This work is supported by Department of Civil Engineering, Faculty of Engineering, Siam University, Thailand.

**Author Contributions:** Plangoen Pheerawat and Parmeshwar Udmale conceived and designed the study; Pheerawat Plangoen analyzed the data; Pheerawat Plangoen and Parmeshwar Udmale wrote the paper.

**Conflicts of Interest:** The authors declare no conflict of interest.

#### References

1. Renard, K.G.; Foster, G.A.; Weesies, G.A.; McCool, D.K.; Yoder, D.C. Predicting Soil Erosion by Water: A Guide to Conservation Planning with the Revised Universal Soil Loss Equation (RUSLE). In *USDA Agriculture Handbook*; Agricultural Research Service: Washington, DC, USA, 1997; No. 703, pp. 400–404.
2. Wischmeier, W.H.; Smith, D.D. Predicting Rainfall Erosion Losses. In *USDA Agricultural Handbook*; Agricultural Research Service: Washington, DC, USA, 1978; No. 537, p. 58.
3. Cohen, M.J.; Shepherd, K.D.; Walsh, M.G. Empirical formulation of the Universal Soil Loss Equation for erosion risk assessment in a tropical watershed. *Geoderma* **2005**, *124*, 235–252. [[CrossRef](#)]
4. Diodato, N. Estimating RUSLE's rainfall factor in the part of Italy with a Mediterranean rainfall regime. *Hydrol. Earth Syst. Sci.* **2004**, *8*, 103–107. [[CrossRef](#)]
5. Diodato, N.; Bellochi, G. Estimating monthly (R)USLE climate input in a Mediterranean region using limited data. *J. Hydrol.* **2007**, *345*, 224–236. [[CrossRef](#)]
6. Angulo-Martínez, M.; Beguería, S. Estimating rainfall erosivity from daily precipitation records: A comparison among methods using data from the Ebro Basin (NE Spain). *J. Hydrol.* **2009**, *379*, 111–121. [[CrossRef](#)]
7. Hernando, D.; Romana, M.G. Estimating the rainfall erosivity factor from monthly precipitation data in the Madrid Region (Spain). *J. Hydrol. Hydromech.* **2015**, *63*, 55–62. [[CrossRef](#)]
8. Fournier, F. *Climate Erosion*; Presses Universitaires de France: Paris, France, 1960.
9. Arnoldous, H.M.J. An approximation of the rainfall factor in the USLE. In *Assessment of Erosion*; De Boodt, M., Gabriels, D., Eds.; Wiley: Chichester, UK, 1980; pp. 127–132.
10. Plangoen, P.; Babel, M.S. Projected Rainfall Erosivity Changes under Future Climate in the Upper Nan Watershed, Thailand. *J. Earth Sci. Clim. Chang.* **2014**, *5*. [[CrossRef](#)]
11. Intergovernmental Panel on Climate Change (IPCC). The physical science basis. In *Contribution of Working Group I to the Fourth Assessment Report of the Intergovernmental Panel on Climate Change*; Solomon, S., Qin, D., Manning, M., Chen, Z., Marquis, M., Averyt, K.B., Tignor, M., Miller, H.L., Eds.; Cambridge University Press: Cambridge, UK, 2007.

12. Neal, M.R.; Nearing, M.A.; Vining, R.C.; Southworth, J.; Pfeifer, R.A. Climate change impacts on soil erosion in Midwest United States with changes in crop management. *CATENA* **2005**, *61*, 165–184. [[CrossRef](#)]
13. Nearing, A.M. Potential changes in rainfall erosivity in the U.S. with climate change during the 21st century. *J. Soil Water Conserv.* **2001**, *56*, 229–232.
14. Zhang, X.C. A comparison of explicit and implicit spatial downscaling of GCM output for soil erosion and crop production assessments. *Clim. Chang.* **2007**, *84*, 337–363. [[CrossRef](#)]
15. Zhang, X.C.; Liu, W.Z. Simulating potential response of hydrology, soil erosion, and crop productivity to climate change in Changwu tableland region on the Loess Plateau of China. *Agric. For. Meteorol.* **2005**, *131*, 127–142. [[CrossRef](#)]
16. Favis-Mortlock, D.T.; Guerra, A.J.T. The implications of general circulation model estimates of rainfall for future erosion: A case study from Brazil. *CATENA* **1999**, *37*, 329–354. [[CrossRef](#)]
17. Mullan, D.; Favis-Mortlock, D.; Fealy, R. Addressing key limitations associated with modelling soil erosion under the impacts of future climate change. *Agric. For. Meteorol.* **2012**, *156*, 18–30. [[CrossRef](#)]
18. Mullan, D. Soil erosion under the impacts of future climate change: Assessing the statistical significance of future changes and the potential on-site and off-site problems. *CATENA* **2013**, *109*, 234–246. [[CrossRef](#)]
19. Plangoen, P.; Babel, M.S.; Clemente, R.S.; Shrestha, S.; Tripathi, N. Simulating the Impacts of Future Land Use and Climate Change on Soil Erosion and Deposition in the Mae Nam Nan Sub-Catchment. *Sustainability* **2013**, *5*, 3244–3274. [[CrossRef](#)]
20. Zhang, Y.-G.; Nearing, M.A.; Zhang, X.-C.; Xie, Y.; Wei, H. Projected rainfall erosivity changes under climate change from multi model and multi scenario projections in Northeast China. *J. Hydrol.* **2010**, *384*, 97–106. [[CrossRef](#)]
21. Shiono, P.; Ogawa, S.; Miyamoto, T.; Kameyama, K. Expected impacts of climate change on rainfall erosivity of farmlands in Japan. *Ecol. Eng.* **2013**, *61*, 678–689. [[CrossRef](#)]
22. Hoomehr, S.; Schwartz, J.S.; Yoder, D. Potential changes in rainfall erosivity under GCM climate change scenarios for the southern Appalachian region, USA. *CATENA* **2016**, *136*, 141–151. [[CrossRef](#)]
23. Panagos, P.; Borrelli, P.; Meusburger, K.; Yu, B.; Klik, A.; Lim, K.J.; Yang, J.E.; Ni, J.; Miao, C.; Chattopadhyay, N.; et al. Global rainfall erosivity assessment based on high-temporal resolution rainfall records. *Sci. Rep.* **2017**, *7*. [[CrossRef](#)] [[PubMed](#)]
24. Zhang, X.C.; Nearing, M.A. Impact of climate change on soil erosion, runoff and wheat productivity in central Oklahoma. *CATENA* **2005**, *61*, 185–195. [[CrossRef](#)]
25. Park, S.; Jin, C.; Choi, C. Predicting soil erosion under land-cover area and climate changes using the revised universal soil loss equation. In *Remote Sensing for Agriculture, Ecosystems, and Hydrology XIII. Proceedings of SPIE*; Neale, C.M.U., Maltese, A., Richter, K., Eds.; Spie-Int Soc Optical Engineering: Bellingham, WA, USA, 2011.
26. Mondal, A.; Khare, D.; Kundu, S.; Meena, P.K.; Mishra, P.K.; Shukla, R. Impact of climate change on future soil erosion in different slope, land use, and soil-type conditions in a part of the Narmada River Basin, India. *J. Hydrol. Eng.* **2015**, *20*. [[CrossRef](#)]
27. Clemente, R.S.; Prasher, S.O.; Barrington, S.F. PESTFADE—A new pesticide fate and transport model: Model development and verification. *Trans. ASAE* **1993**, *36*, 357–367. [[CrossRef](#)]
28. Panagos, P.; Meusburger, K.; Ballabio, C.; Borrelli, P.; Beguería, S.; Klik, A.; Rymaszewicz, A.; Michaelides, S.; Olsen, P.; Tadić, M.P.; et al. Reply to the comment on “Rainfall erosivity in Europe” by Auerswald et al. *Sci. Total Environ.* **2015**, *532*, 853–857. [[CrossRef](#)] [[PubMed](#)]
29. Oliveira, P.T.S.; Wendland, E.; Nearing, M.A. Rainfall erosivity in Brazil: A review. *Catena* **2013**, *100*, 139–147. [[CrossRef](#)]
30. Prasannakumar, V.; Vijith, H.; Abinod, S.; Geetha, N. Estimation of soil erosion risk within a small mountainous sub-watershed in Kerala, India, using Revised Universal Soil Loss Equation (RUSLE) and geo-information technology. *Geosci. Front.* **2012**, *3*, 209–215. [[CrossRef](#)]
31. Land Development Department (LDD). *Group of Soil Series for Economic Crops of Thailand*; Office of Soil Survey and Land use Planning, Ministry of Agriculture and Cooperatives: Bangkok, Thailand, 2005. (In Thai)
32. Southeast Asia START Regional Center (SEA START). *Southeast Asia Regional Vulnerability to Changing Water Resource and Extreme Hydrological Events due to Climate Change*; Technical Report No. 15; Southeast Asia START Regional Centre: Bangkok, Thailand, 2006.
33. Land Development Department (LDD). *Soil Series Map Scale 1:25,000*; Land Development Department. Ministry of Agriculture and Cooperatives: Bangkok, Thailand, 2007.

34. Land Development Department (LDD). *Soil Erosion in Thailand*; Ministry of Agriculture and Cooperatives: Bangkok, Thailand, 2002. (In Thai)
35. Foster, G.R.; Toy, T.E.; Renard, K.G. Comparison of the USLE, RUSLE1.06c, and RUSLE2 for application to highly disturbed lands. In Proceedings of the 1st Interagency Conference on Research in the Watersheds, Benson, AZ, USA, 27–30 October 2003.
36. Brown, L.C.; Foster, G.R. Storm erosivity using idealized intensity distributions. *Trans. ASAE* **1987**, *30*, 379–386. [[CrossRef](#)]
37. McSweeney, C.F.; Jones, R.G.; Lee, R.W.; Rowell, D.P. Selecting CMIP5 GCMs for downscaling over multiple regions. *Clim. Dyn.* **2015**, *44*, 3237–3260. [[CrossRef](#)]
38. Fowler, H.J.; Blenkinsop, S.; Tebald, C. Linking climate change modelling to impacts studies: Recent advances in downscaling techniques for hydrological modeling. *Int. J. Climatol.* **2007**, *27*, 1547–1578. [[CrossRef](#)]
39. Gudmundsson, L.; Bremnes, J.B.; Haugen, J.E.; Engen-Skaugen, T. Technical Note: Downscaling RCM precipitation to the station scale using statistical transformations—A comparison of methods. *Hydrol. Earth Syst. Sci.* **2012**, *16*, 3383–3390. [[CrossRef](#)]



© 2017 by the authors. Licensee MDPI, Basel, Switzerland. This article is an open access article distributed under the terms and conditions of the Creative Commons Attribution (CC BY) license (<http://creativecommons.org/licenses/by/4.0/>).